Microwave Imaging behind a Drywall using Synthetic Aperture Radar

Alireza Ghobadi-Rad, Majid Tayarani
Electrical Engineering, University of Science and Technology, Narmak, Tehran, Iran
a_ghobadi@elec.iust.ac.ir, m_tayarani@iust.ac.ir
Corresponding author: m_tayarani@iust.ac.ir

Abstract- **We study through a drywall imaging using synthetic aperture radar (SAR) method. Transmission and reflection characteristics of the wall are analyzed by a rigorous coupled-wave analysis (RCWA) method. The Bragg modes are investigated on analytic formulation and reconstructed image. The cutoff frequency for different Bragg modes is calculated and the relative power carried by each of these modes is shown. The Green function of such a periodic structure is derived by representing a line source radiation in the spectral domain. The analytical results are then validated by the numerical FEM results using the COMSOL software and the effect of the number of the Bragg modes is shown. Having numerically calculated backscattered fields of a target behind the wall and the free-space Green function, the SAR image of the target is computed and the image artifacts due to the presence of the wall are addressed. Firstly, we show that the target image is still distorted and not focused even with the background subtraction. Secondly, by properly employing the phase of the wall Green function instead of the free-space Green function, we indicate that the target image is successfully refocused.**

Index Terms- microwave imaging, Green function, periodic structure, Bragg modes.

I. INTRODUCTION

THROUGH-the-Wall Imaging (TWI) is the ability to detect and image target behind wall by using electromagnetic (EM) waves. This type of technology is highly desirable in search-and-rescue mission, behind-wall target detection, and surveillance and reconnaissance in urban environments [1]-[3]. Direct reflection from wall is a strong clutter which limit the dynamic range of the imaging receiver. To solve this problem, frequency and time domain filtering is proposed in [5]-[7]. Imaging refocusing by a matched filtering techniques for homogeneous wall is investigated in [4]. Extending the method of [4] to an inhomogeneous cinder block wall, the target image was refocused using a proper matched filter in [8]. For calculation of GF in [8], modal analysis method is used according to
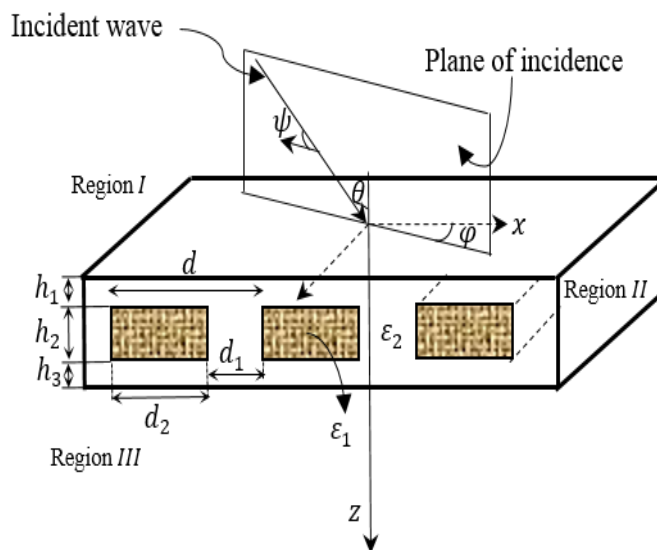
Fig. 1. Geometry of the drywall structure illuminated by an obliquely incident plane wave. Let us assume the structure parameters as follows. $d_2 = 12\ cm$, $d_1 = 3\ cm$, $h_2 = 16\ cm$ and $h_1 = h_3 = 2\ cm$

[9]. In [9] by using modal analysis, the cinder block wall is modeled by a periodic multilayer structure. The study was limited to only transverse electric (TE) polarization and large number of Bragg modes was not investigated in [9] due to matrix inversion complexities.

The 3D oblique illumination of a one layer periodic structure by using the rigorous coupled-wave analysis (RCWA) is investigated in [10]. RCWA technique [10] is an effective method that is not limited to the specific TE polarization and more importantly, the large number of the Bragg modes does not impose any issue on it. Here, we compute the Green's function (GF) of the periodic drywall using extended one layer binary grating layer to multilayer periodic structure by RCWA technique [10]. Then we use the back projection method (BPM) [4] and the proper GF to reconstruct concealed targets images.

In Section II, by using the RCWA method and extended to drywall structures, in forward scattering problem, the cutoff frequency is calculated and the relative power carried by each of Bragg modes are shown. Transmission (T), reflection (R) and GF calculation is presented and RCWA analysis results are validated by those of finite element method (FEM) of COMSOL.

In Section III, the effects of a drywall on the target image are investigated to observe some challenges. The modified BPM that employs the phase of the wall Green function yields a focused image. Section IV concludes this paper.
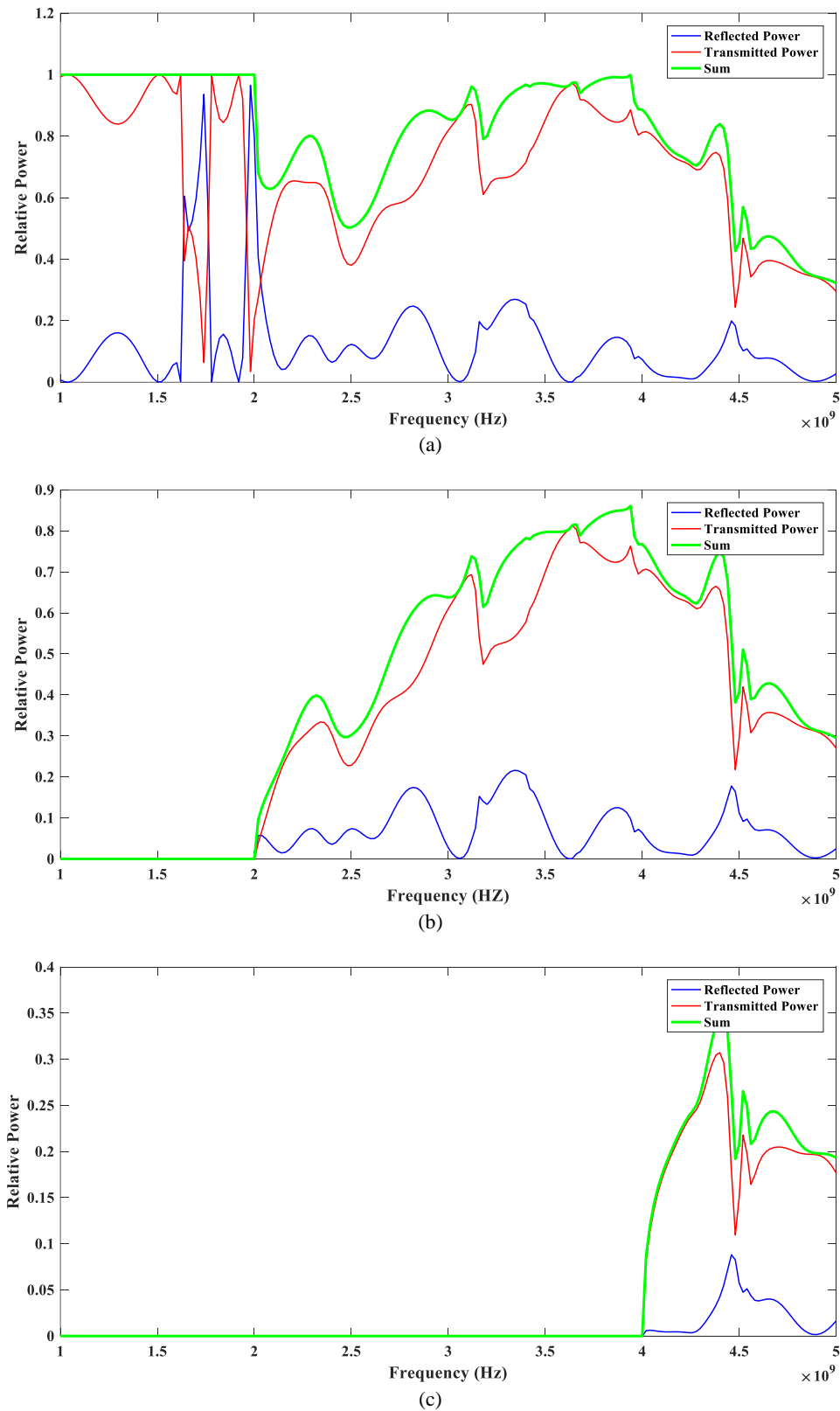
Fig. 2. Relative power carried with Bragg modes, (a) $n = 0$, (b) $n = \pm 1$, (c) $n = \pm 2$

.

II. DRYWALL ANALYSIS USING RCWA

The three-layer structure of Fig. 1, that is periodic along the x-axis, models a drywall. The wooden sheet of h_2 thickness are placed between free space layers with thicknesses h_1 and h_3. Complex relative permittivity of the wooden layers are assumed $\varepsilon_1 = \varepsilon_1' + j\varepsilon_1''$ and free space permittivity is $\varepsilon_2 = 1$. Periodicity of the structure is $d = d_1 + d_2$, where d_1 and d_2 are shown in Fig. 1. As shown in Fig. 1, linear polarized electromagnetic wave is obliquely incident on the structure at an arbitrary angle of incidence θ with respect to the z-axis and at an azimuth angle φ with respect to the x-axis. ψ is the angle between the electric-field vector and the plane of incidence. $\psi = 0$ and $\psi = 90$ denotes transverse magnetic (TM) and transverse electric (TE) polarization, respectively

A. Relative power calculation

A computer code in MATLAB has been developed to calculate the relative power of the drywall using RCWA method. The details of derivations are addressed in Appendix A. According to Fig. 1, the structure parameters are $h_2 = 16cm, d = 15cm, h_1 = h_3 = 2cm$. The dielectric constant of wooden sheets are $\varepsilon_1 = 2.4$.

According to Appendix A, relative power for TE polarization wave and $\theta = \varphi = 0$ in the frequency interval 1-3 GHz is shown in Fig. 2. According to Fig. 2(a) the only propagation mode up to 2 GHz is $n = 0$ and sum of reflected power and transmitted power to incident power is one. As the frequency increases, this ratio decreases and due to the propagation of higher order Bragg modes, the sum of these relative powers are not one. In Fig. 2(b) and Fig. 2(c) relative power for higher order modes $n = \pm 1$ and $n = \pm 2$ are shown respectively.

B. Scattering parameter and Green Function

To calculate scattered fields, a Gaussian beam with width $\omega_0 = 0.2\,m$ is illuminating the structure normally. We expand the Gaussian beam into spectrum of plane waves and then compute response of the structure to each of the plane waves, and finally employ superposition [11]. Thus, we reach to the following reflected and transmitted fields

$$E_y^{ref/tra}(x, x', z, z', k)$$

$$= \frac{1}{2\pi}\omega_0\sqrt{\pi}\int_{-\infty}^{+\infty}\sum_n \mathcal{F}_n(k, k_x)\,e^{-k_x^2\frac{\omega_0^2}{4}}\,e^{-jk_{z_n}z-jk_zz'+jk_{x_n}x-jk_xx'}\,dk_x \qquad (1)$$

$$k_{x_n} = k_x + \frac{2\pi}{d}n \qquad k_{zn} = \sqrt{k^2 - k_{x_n}^2} \qquad (2)$$

where $\mathcal{F}_n(k, k_x)$ is the reflection or transmission coefficients (reviewed in Appendix A) of the nth
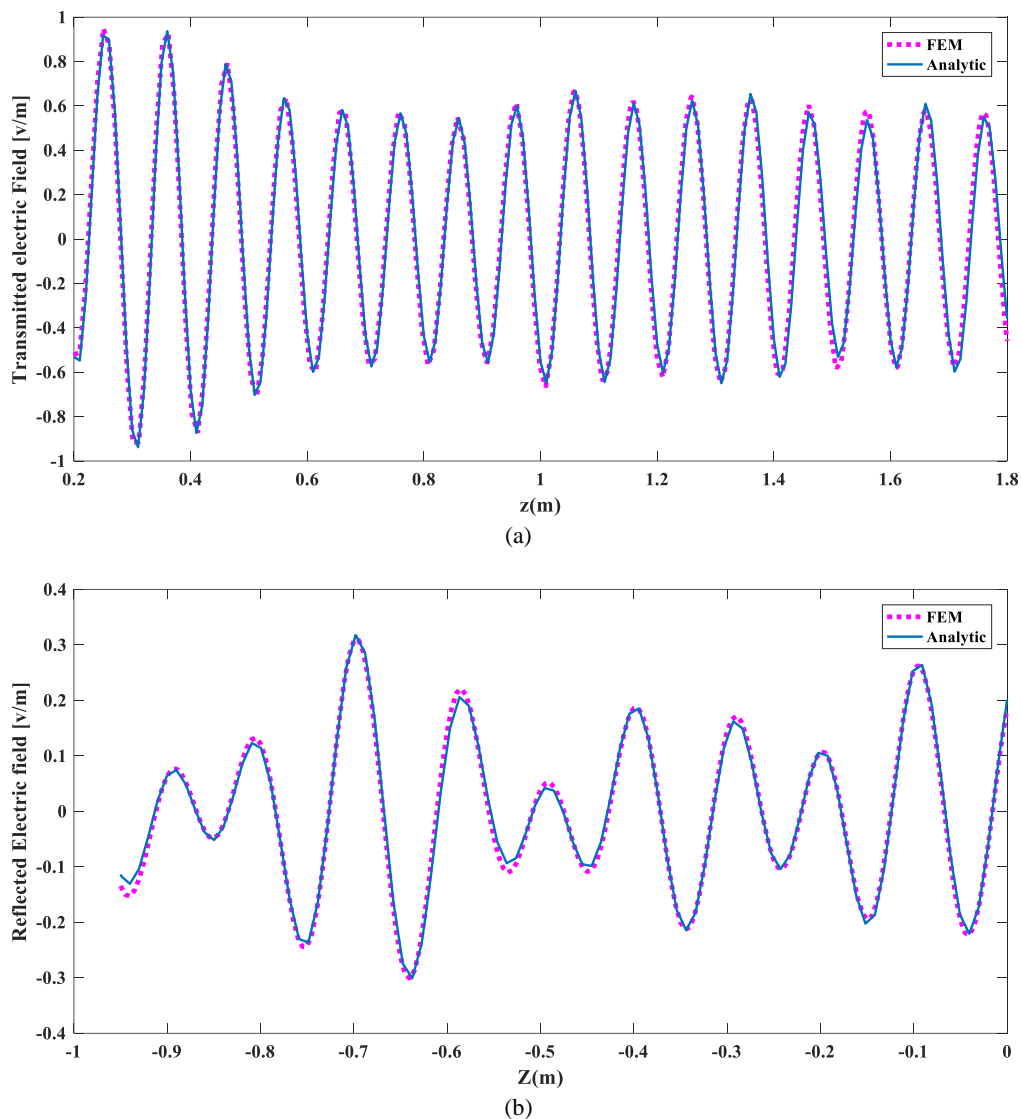
Fig. 3. Comparison of the analytic and numerical (FEM) results of reflected and transmitted fields.
(a) Transmitted Field, (b) Reflected Field

Bragg mode. For validation of this development, we compare our code results with those of the finite element method (FEM) of COMSOL software. Fig. 3 shows the results of reflection (R) and transmission (T) coefficients, probed at the middle line $x = 0$ and for $-0.95m \leq z \leq 1.2$ at frequency 3 GHz. good agreement is achieved between analytic formulation and the FEM numerical results by increasing the number of modes.

For GF calculation, according to Fig. 1, we consider a line source, parallel to the y-axis in the wall front ($z < 0$). We estimate the GF by computing the line source radiated field which is proportional to the Hankel function of the second kind (using $e^{j\omega t}$ time convention). We expand the line source radiated fields (cylindrical waves) into plane waves [11]. It is well known that each plane wave generates several Bragg modes. The number and direction of each Bragg mode depends on the wavenumber k and direction of the incident plane wave θ. Thus, by calculating the following
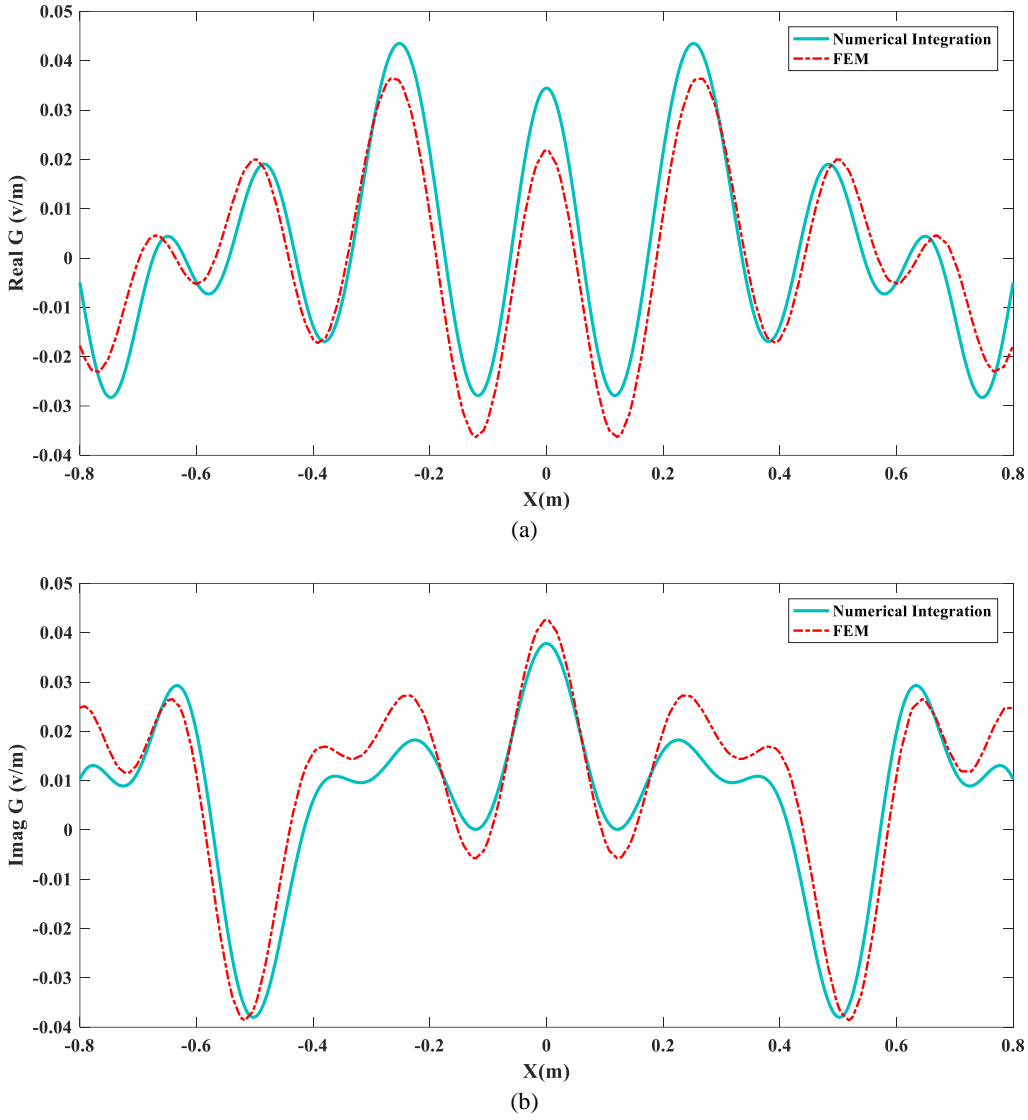
Fig. 4. The Green function of the structure: (a) real part and (b) imaginary part.

numerical integral, the Green function is determined

$$G(x,x',z,z',k) = -\frac{1}{4\pi j} \int\limits_{-\infty}^{+\infty} \sum_{n} t_n(k,k_x) \frac{e^{-jk_{z_n}z+jk_zz'}}{k_z} e^{-jk_{x_n}x+jk_xx'} dk_x \qquad (3)$$

where $t_n(k,k_x)$ is the transmission coefficient of the nth Bragg mode at the frequency f where $k = 2\pi f/c$, c is the speed of light in free-space and the wavenumber along x is k_x. To validate the results of (3), we have compared them with the FEM results of COMSOL. The structure in Fig. 1 is illuminated by a line source, placed at $z = -0.95\ m$ and $x = 0$. The real and imaginary parts of the Green function at the point $z = 0.7m$ for different x values, within the interval of $[-0.6m, 0.6m]$ are shown in Fig. 4(a) and Fig. 4(b), respectively. According to Fig. 4, a good agreement between numerical integration and FEM results has been achieved.

III. IMAGING

A. Imaging scenario

We construct the 2D image of a conducting cylinder with a radius of 10 cm behind the wall at $z_t = 0.8\ m$. The wall parameters are the same as those in the caption of Fig. 1 and it is illuminated by a TE polarized wave propagating in the xz-plane. The first step for this purpose is collecting scattered fields from the target behind the wall that is carried out using FEM of COMSOL software. Ultra wideband antenna working within the frequency interval of $1 - 3$ GHz moves along a scan line of length $L = 1.2\ m$ along the x direction and collects backscattered fields at different frequency and observation points. The scan line is chosen to be parallel to the wall, placed at $z_{antenna} = -0.95 m$. Using the standard BPM, the target image is computed by [4]

$$S(\vec{r}) = \frac{1}{N_p N_f} \sum_{m=1}^{N_f} \sum_{n=1}^{N_p} E_y(\vec{r}_n, k_m) R_n^2(\vec{r}_n, \vec{r})\ e^{2jk_m R_n(\vec{r}_n, \vec{r})} \tag{4}$$

where $E_y(r_n, k_m)$ is either the total received field or the background subtracted field, probed at $r_n = (x_n, z_n)$ and $k_m = 2\pi f_m/c$ is the wave constant at the mth frequency point f_m. Here, $R_n(r_n, r) = |r_n - r|$ is the distance from the nth observation point. Considering the 25 MHz frequency step size, the number of frequency points is $N_f = 81$. In addition, the number of observation points N_p is 51, if the transceiver moves by 2.4 cm step within the x interval of -0.6 m to $+0.6$ m.

The target image is calculated and plotted in Fig. 5. Fig. 5(a) shows the background image demonstrating large reflections from the wall. This background can even mask some objects. Here, we use the background subtraction technique to eliminate the wall effect and extract the image of the behind-the-wall object only. Figs. 5(b) shows the complete scenario image and Fig. 5(c) shows the background subtracted image of the target (i.e. the behind-the-wall object only). As shown the target image is deteriorated and not clear. This stems from the fact that waves propagate through an inhomogeneous and periodic wall and this makes images unfocused. Basically, we expected to have only a focused point at a, but other points (b, c, d and e) are also emerged.

B. Proper Green Function

The Green function of the drywall is addressed in section II.B. To remove artifacts from the image (Fig. 5), we use only the phase of the Green function [4]. The new imaging formulation is given by
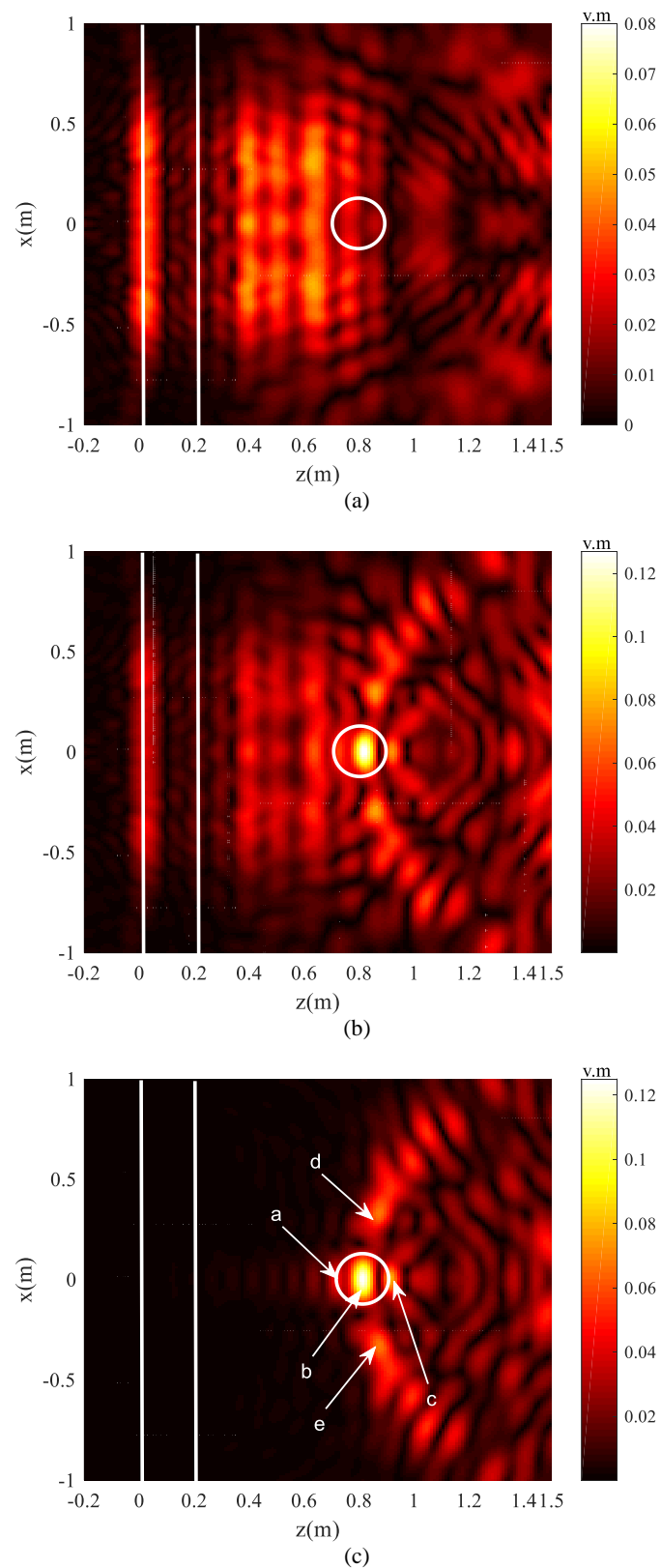
Fig. 5. The standard back projection images for different cases: (a) the drywall alone, (b) the metallic target behind the drywall, (c) the target-behind-the-wall alone (i.e. background subtraction is performed)
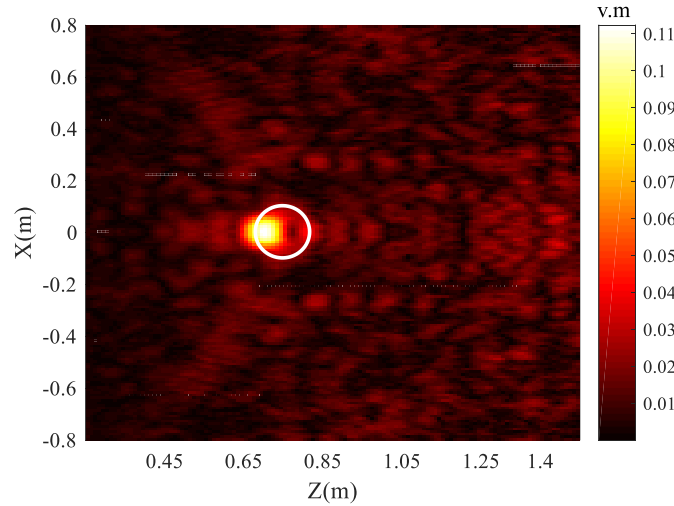
Fig. 6. The Refocused image of the target using phase of the proper GF. Background subtraction is performed.

$$S(\vec{r}) = \frac{1}{N_p N_f} \sum_{m=1}^{N_f} \sum_{n=1}^{N_p} E_y(\vec{r_n}, k_m) R_n^2(\vec{r_n}, \vec{r}) \, e^{2j\angle G(\vec{r_n}, \vec{r}, k_m)} \tag{5}$$

where $\angle G(r_n, r, k_m)$ is the phase of the GF, once the source is located in the wall front ($z < 0$) and observation point is in the wall back ($z > 0.2m$). Employing (5), we image the target and show the result after background subtraction technique in Fig. 8. Compared to Fig. 5(c), it is evident that by using the phase of the GF, exact location is obtained and unrealistic images are eliminated.

IV. CONCLUSION

In order to obtain a properly refocused image of a target behind a drywall, a proper estimation of the structure GF is necessary. In this paper, by using RCWA, transmission and reflection coefficients for drywall are calculated accurately and the GF is correctly estimated. . The cutoff frequency for different Bragg modes is calculated and the relative power carried by each of these modes is shown. By properly employing the phase of the wall Green function instead of the free-space Green function, we indicate that the target image is successfully refocused.

APPENDIX

In region I, the incident electric-field vector is

$$E_{inc} = \hat{u} \, \exp[-jk(\sin\theta \cos\varphi \, x + \sin\theta \sin\phi \, y + \cos\theta \, z)] \tag{6}$$

Where $k = 2\pi/\lambda$ and λ is the wavelength of the incident wave in free space (assuming the

refractive index n_1 of the region I is1), and assuming$\psi = \pi/2$, the polarization unit vector $\hat{u}$ is

$$\hat{u} = -sin\phi\hat{x} + cos\varphi\,\hat{y} \tag{7}$$

The total vector electric field in the region I ($z < 0$) and in region III ($z > 0.2m$) are expressed as [10]

$$E_{\mathrm{I}} = E_{inc} + \sum_i R_i \exp\left[-j(k_{xi}x + k_y y - k_{1,zi}z)\right] \tag{8}$$

$$E_{\mathrm{III}} = \sum_i T_i \exp\left\{-j[k_{xi}x + k_y y + k_{\mathrm{III},zi}(z - 2 \times h_1 - h_2)]\right\} \tag{9}$$

where

$$k_{xi} = k\,sin\theta\,cos\varphi - \frac{2\pi i}{d} \qquad (i = \cdots - 1,0,1 \cdots) \tag{10}$$

$$k_y = k\,sin\theta\,sin\varphi \tag{11}$$

$$k_{\ell,zi} = \begin{cases} ((k_\ell)^2 - k_{xi}{}^2 - k_y{}^2)^{\frac{1}{2}} & (k_{xi}^2 + k_y^2) < (k_\ell)^2 \\ -j(k_{xi}{}^2 + k_y{}^2 - (k_\ell)^2)^{\frac{1}{2}} & (k_{xi}^2 + k_y^2) > (k_\ell)^2 \end{cases} \tag{12}$$

Here, $k_{\ell,zi}$ is wavenumber of a propagating wave or an evanescent wave, R_i is the magnitude of the ith reflected wave in region I, and T_i is the magnitude of the ith transmitted wave in region III. In each ℓth layer of region II, the fields may be expressed as a Fourier expansion in terms of space harmonic fields [10]

$$E_\ell = \sum_i \left[S_{\ell xi}(z)x + S_{\ell yi}(z)y + S_{\ell zi}(z)z\right] \times \exp\left[-j(k_{xi}x + k_y y)\right] \tag{13}$$

$$H_\ell = -j\left(\varepsilon_0/\mu_0\right)^{\frac{1}{2}}\Sigma_i\left[U_{\ell xi}(z)x + U_{\ell yi}(z)y + U_{\ell zi}(z)z\right] \times \exp\left[-j(k_{xi}x + k_y y)\right] \tag{14}$$

Where $S_{\ell i}(z)$ and $U_{\ell i}(z)$ are the magnitudes of the ith space-harmonic fields E_ℓ and H_ℓ that satisfy Maxwell's equations in the ℓth layer of region II. That is, we have

$$\nabla \times E_\ell = -j\omega\mu_0 H_\ell \quad \nabla \times H_\ell = -j\omega\varepsilon_0\varepsilon_\ell(x)E_\ell \tag{15}$$

Where $\varepsilon_\ell(x)$ is the relative permittivity of the ℓ^{th}layer and is expressed by a periodic function and expanded by a Fourier series. Substituting (13) and (14) into (15) and eliminating the normal components of the field, we obtain the set of coupled-wave equations in the following matrix form

$$
\begin{bmatrix} \dot{S}_{\ell,y} \\ \dot{S}_{\ell,x} \\ \dot{U}_{\ell,y} \\ \dot{U}_{\ell,x} \end{bmatrix} = \begin{bmatrix} 0 & 0 & K_y\mathcal{E}_\ell^{-1}K_x & I - K_y\mathcal{E}_\ell^{-1}K_y \\ 0 & 0 & K_x\mathcal{E}_\ell^{-1}K_x - I & -K_x\mathcal{E}_\ell^{-1}K_y \\ K_xK_y & \mathcal{E}_\ell - K_y^2 & 0 & 0 \\ k_x^2 - \mathcal{E}_\ell & -K_xK_y & 0 & 0 \end{bmatrix} \begin{bmatrix} S_{\ell,y} \\ S_{\ell,x} \\ U_{\ell,y} \\ U_{\ell,x} \end{bmatrix} \tag{16}
$$

Where K_y and K_x are diagonal matrices with the elements k_y/k_0 andk_{xi}/k_0, respectively. Here, $\mathcal{E}_\ell$ is the matrix formed by the permittivity harmonic component$\varepsilon_{\ell,ip} = \varepsilon_{\ell,i-p}$. Equation (16) in a compact form is

$$
\dot{V}_\ell = A_\ell V_\ell \tag{17}
$$

Where V_ℓ is a vector composed of $S_{\ell,x}$, $S_{\ell,y}$, $U_{\ell,x}$ and $U_{\ell,y}$ and dot represents differentiation with respect to z.

The coefficient matrix A_ℓ is a system matrix composed of the 16 sub-matrices in (16) that are in turn specified by the 4 sets of coupled-wave equations. Equation (17) may be solved using a state-variable method by calculating the eigenvalues and eigenvectors associated with the matrix A_ℓ [10].

The solution of the $S_{\ell,x}$, $S_{\ell,y}$, $U_{\ell,x}$, $U_{\ell,y}$ using the state variable method [12] is

$$
S_{\ell,xi}(z) = \sum_m C_{\ell m} w_{\ell,1,im} exp(\lambda_{\ell m}z) \tag{18}
$$

$$
S_{\ell,yi}(z) = \sum_m C_{\ell m} w_{\ell,2,im} exp(\lambda_{\ell m}z) \tag{19}
$$

$$
U_{\ell,xi}(z) = \sum_m C_{\ell m} w_{\ell,3,im} exp(\lambda_{\ell m}z) \tag{20}
$$

$$
U_{\ell,yi}(z) = \sum_m C_{\ell m} w_{\ell,4,im} ex\, p(\lambda_{\ell m}z) \tag{21}
$$

where $C_{\ell m}$'s are the unknown constants to be determined by applying boundary conditions, $\lambda_{\ell m}$'s are the eigenvalues of the matrix A_ℓ, and $w_{\ell,q,im}$'s are the elements of the eigenvector matrices

corresponding to a given value of i.

To compute the reflected and transmitted field in the region I and III, the tangential electric and magnetic fields at two sides of each boundary are matched. The resulting system of equations are solved for the values R_i and T_i. At $z = 0$, we have

$$u_x \delta_{i0} + R_{xi} = S_{Ixi}(0) \tag{22}$$

$$u_y \delta_{i0} + R_{yi} = S_{Iyi}(0) \tag{23}$$

$$u_z k_y \delta_{i0} - u_y k_{I,zi} \delta_{i0} + k_{I,zi} R_{yi} + k_y R_{zi} = U_{Ixi}(0) \tag{24}$$

$$u_x k_{I,zi} \delta_{i0} - u_z k_{xi} \delta_{i0} - k_{I,zi} R_{xi} - k_{xi} R_{zi} = U_{Iyi}(0) \tag{25}$$

At $z = h_1$, we have
$$S_{Ixi}(h_1) = S_{IIxi}(h_1) \tag{26}$$

$$S_{Iyi}(h_1) = S_{IIyi}(h_1) \tag{27}$$

$$U_{Ixi}(h_1) = U_{IIxi}(h_1) \tag{28}$$

$$U_{Iyi}(h_1) = U_{IIyi}(h_1) \tag{29}$$

At $z = h_1 + h_2$, we have

$$S_{IIxi}(h_1 + h_2) = S_{IIIxi}(h_1 + h_2) \tag{30}$$

$$S_{IIyi}(h_1 + h_2) = S_{IIIyi}(h_1 + h_2) \tag{31}$$

$$U_{IIxi}(h_1 + h_2) = U_{IIIxi}(h_1 + h_2) \tag{32}$$

$$U_{IIyi}(h_1 + h_2) = U_{IIIyi}(h_1 + h_2) \tag{33}$$

At $z = h_1 + h_2 + h_3$, we have
$$S_{IIIxi}(h_1 + h_2 + h_3) = T_{xi} \tag{34}$$

$$S_{\text{III}yi}(h_1 + h_2 + h_3) = T_{yi} \tag{35}$$

$$U_{\text{III}xi}(h_1 + h_2 + h_3) = -k_{\text{III},zi}T_{yi} + k_y T_{zi} \tag{36}$$

$$U_{\text{III}yi}(h_1 + h_2 + h_3) = k_{\text{III},zi}T_{xi} - k_{xi}T_{zi} \tag{37}$$

For a plane wave illumination, we have

$$k_{xi}R_{xi} + k_y R_{yi} - k_{\text{I},zi}R_{zi} = 0 \tag{38}$$

$$k_{xi}T_{xi} + k_y T_{yi} + k_{\text{III},zi}T_{zi} = 0 \tag{39}$$

By rewriting Eqs. (22) - (39) in matrix forms, we obtain

$$\begin{bmatrix} u_x \delta_{i0} \\ u_y \delta_{i0} \\ u_z k_y \delta_{i0} - u_y k_{\text{I},zi}\delta_{i0} \\ u_x k_{\text{I},zi}\delta_{i0} - u_z k_{xi}\delta_{i0} \end{bmatrix} + \begin{bmatrix} I & 0 & 0 \\ 0 & I & 0 \\ 0 & k_{\text{I},zi} & k_y \\ -k_{\text{I},zi} & 0 & -k_{xi} \end{bmatrix}\begin{bmatrix} R_x \\ R_y \\ R_z \end{bmatrix} = [Q_{1m}(0)][C_{1m}] \tag{40}$$

$$[Q_{1m}(h_1)][C_{1m}] = [Q_{2m}(h_1)][C_{2m}] \tag{41}$$

$$[Q_{2m}(h_1 + h_2)][C_{2m}] = [Q_{3m}(h_1 + h_2)][C_{3m}] \tag{42}$$

$$[Q_{3m}(h_1 + h_2 + h_3)][C_{3m}] = \begin{bmatrix} I & 0 & 0 \\ 0 & I & 0 \\ 0 & -k_{\text{III}zi} & k_y \\ k_{\text{III},zi} & 0 & k_{xi} \end{bmatrix}\begin{bmatrix} T_x \\ T_y \\ T_z \end{bmatrix} \tag{43}$$

where

$$Q_{\ell m}(z) = w_{\ell,q,m}\ exp(\lambda_{\ell m}z) \tag{44}$$

By using a technique to eliminate common matrices and to solve linear equations simultaneously, we can find **T** and **R** coefficients [12].

REFERENCES

[1]   M. G. Amin, Through-the-Wall Radar Imaging FL, US, CRC Press, 2010.

[2]   M. Amin and K. Sarabandi, "Special issue on remote sensing of building interior," *IEEE Trans. Geosci. Remote Sens.*, vol. 47, no.5, pp. 1267-1368, May. 2009.

[3]   L. Li, W. Zhang, and F. Li, "A novel autofocusing approach for realtime through-wall imaging under unknown wall characteristics," *IEEE Trans. Geosci. Remote Sens.*, vol. 48, no.1, pp. 423-431, Jan. 2010.

[4]   M. Dehmollaian and K. Sarabandi, "Refocusing through building walls using synthetic aperture radar*" IEEE Trans. Geosci. Remote Sens.*, vol. 46, no. 6, pp. 1589–1599, Jun. 2008.

[5]   R. Solimene and A. Cuccaro, "Front Wall Clutter Rejection Methods in TWI," *IEEE Geoscience and Remote Sensing Letters.*, vol. 11, no. 6, pp. 1158 - 1162, June 2014.

[6]   B. Yektakhah and M. Dehmollaian, "A Method for Cancellation of Clutter Due to an Object in Transceiver Side of a Wall for Through-Wall Sensing Application," *IEEE Geoscience and Remote Sensing Letters*, vol. 9, no. 4, pp. 559- 563, July 2012.

[7]   Y.-S. Yoon and M. G. Amin, "Spatial filtering for wall-clutter mitigation in through-the-wall radar imaging," *IEEE Trans. Geosci. Remote Sens.*, vol. 47, no. 9, pp. 3192–3208, Sep. 2009.

[8]   V.Khorashadi-zadeh and M. Dehmollaian, "Through a Cinder Block Wall Refocusing Using SAR Back Projection Method," *IEEE Trans. Antennas Propag.*, vol.67, no. 1, pp. 1212–122, Feb.2019.

[9]   W. Honcharenko, H. L. Bertoni. "Transmission and reflection characteristics at concrete block walls in the UHF bands proposed for future PCS," *IEEE Trans. Antennas and Propag.,* vol. 42, no. 2, pp. 232-9, Feb. 1994.

[10] M. G. Moharam, E. B. Grann, and D. A. Pommet, "Formulation for stable and efficient implementation of the rigorous coupled-wave analysis of binary gratings," *J. Opt. Soc. Amer. A,* vol. 12, pp. 1068–1076, May. 1995.

[11] D. G. Dudley, Mathematical foundations for electromagnetic theory. NY, United States, IEEE press, 1994.

[12] Liu, E.g.C.L. Liu, J.W.S.: 'Linear Systems Analysis'. (McGraw-Hill, New York 1975)